A comparison of third and second order accurate finite volume schemes for the two-dimensional compressible Euler equations

Sebastian Noelle

Abstract. We develop, implement and test a new third order accurate MUSCL type finite volume scheme for the two-dimensional Euler equations of compressible fluid flow and compare the scheme with an anlogous second order scheme. It turns out that for many applications the third order scheme is less efficient than the second order one.

AMS Classification Code: 65-05, 65M06, 76L05

Keywords: High order accurate finite volume schemes, multi-dimensional reconstruction and limiting, comparison of efficiency

1. Introduction

For **one-dimensional** scalar conservation laws, several TVB (total-vatiation-bounded) schemes have recently been derived which which may be interpreted as MUSCL-type finite difference schemes [11, 4, 7].

In this paper we present a new third order MUSCL-type finite volume scheme built upon an inherently **multidimensional** spatial reconstruction and limiting procedure. We present a careful comparison of the stability, accuracy, and efficiency of our third order scheme and an analogous second order scheme for a variety of test problems involving plane waves oblique to the grids, a radially symmetric flow with strong shocks and the double mach reflection problem.

Even though the third order scheme often gives somewhat smaller errors, it is in most cases not as efficient as the corresponding second order scheme. These results cast a doubt on the future of higher than second order multi-dimensional MUSCL-type finite difference and finite volume schemes, which were so strongly advocated by several authors who developed them in the one-dimensional context.

2. A class of second and third order accurate MUSCL-type finite volume schemes for the two-dimensional Euler equations

Let us sketch the buildingblocks of the third order scheme: In order to test the scheme in a well-defined context, we implement it on uniform cartesian and hexagonal grids. Hexagonal grids are the most isotropic grids in two space dimensions. The finite volume fluxes which leave a hexagonal cell across its sides influence all neighboring cells, while for a cartesian grid, the corner cells are neglected.

The next choice to be made is the coordinate frame in the space of dependent variables in which we want to perform the multi-dimensional reconstruction and limiting. We rule out characteristic variables, because they are based upon a one-dimensional diagonalization of the system. Conservative variables (ρ, m, n, e) (density, momentum and total energy) have the property that the discrete values $\bar{U}_K$ represent cell averages of the conserved quantities over cell K. This makes them natural candidates for higher than second order schemes, where the reconstruction is not piecewise linear anymore, and one has to distinguish carefully between cell averages and point values at the cell center. On the other hand, the primitive variables (ρ, u, v, p) have desirable properties as well: limiting the spatial reconstruction in these variables guarantees a nonnegative internal energy in the spatial reconstruction. Moreover, velocities and pressure remain constant across a contact discontinuity, while all components of the conservative variables have jumps across such waves.

We combine the advantages of conservative and primitive variables by the following procedure: In a first step, we derive a two-dimensional piecewise quadratic central reconstruction of the conservative variables over cell K based on given cell averages. From this, we obtain a reconstruction of the primitive variables by matching the coefficients of a quadratic expansion of these variables with those of the conservative variables. If, for example, quadratic reconstructions $\tilde{\rho}_K(x,y), \tilde{m}_K(x,y), \tilde{n}_K(x,y), \tilde{e}_K(x,y)$ of density, momentum and energy are given, we define the quadratic reconstructions $\tilde{u}_K(x,y), \tilde{v}_K(x,y), \tilde{p}_K(x,y)$ of the primitive variables by prescribing that for all $(x,y) \in K$,

$$\begin{aligned}
\tilde{\rho}_K(x,y)\,\tilde{u}_K(x,y) &= \tilde{m}_K(x,y) + O(h^3),\\
\tilde{\rho}_K(x,y)\,\tilde{v}_K(x,y) &= \tilde{n}_K(x,y) + O(h^3),\\
\frac{1}{\gamma-1}\tilde{p}_K(x,y) + \frac{1}{2}\tilde{\rho}_K(x,y)\left(\tilde{u}_K(x,y)^2 + \tilde{v}_K(x,y)^2\right) &= \tilde{e}_K(x,y) + O(h^3),
\end{aligned}$$

where $h = \sqrt{K}$ denotes the grid size. This will lead to a third order accurate reconstruction in primitive variables.

In the next step, we limit this reconstruction. Let $\bar{V}_K$ be the vector of primitive variables corresponding to the cell averages $\bar{U}_K$ of the conservative variables, and suppose that $\tilde{\phi}_K(x,y)$ is a given quadratic reconstruction of the primitve variables over cell K. Then the limited reconstruction is given by

$$\phi_K(x,y) := \alpha\,\tilde{\phi}_K(x,y) + (1-\alpha)\,\bar{V}_K,$$

where $\alpha \in [0,1]$ is the largest number such that at all quadrature points $(x_l, y_l) \in \partial K$,

$$\min_{K' \cap K \neq \emptyset} \bar{V}_{K'} \leq \phi_K(x_l, y_l) \leq \max_{K' \cap K \neq \emptyset} \bar{V}_{K'}$$

holds componentwise. This limiting procedure is inherently multidimensional. It does not enforce any monotonicity constraints on the reconstruction, and the piecewise quadratic reconstruction is allowed to possess extrema in the interior of the cell K. It is remarkable that such a weak form of a limiter leads to a stable scheme even in the presence of strong shocks.

In order to obtain accuracy in time, we extrapolate the spatial reconstruction over each cell using the differential equation. For problems involving strong shocks, this should be done locally at a quadrature point in order to avoid nonphysical values. In our experience, time-extrapolation yields faster codes and more accurate results than a Runge-Kutta timestep iteration. The scheme is completed by applying an approximate Riemann solver at the quadrature points, using two-point Gaussian quadrature both in space and time. For further details see [10].

3. Numerical experiments

In the following, we present a detailed comparison of the new third order schemes on cartesian and hexagonal grids with corresponding standard second order schemes.

3.1. Oblique Smooth Flow

We begin with a plane sine wave travelling obliquely across the two-dimensional grids. The experimental orders of convergence (EOC) converge neatly towards 3.0 for the unlimited third order scheme both in L^1- and L^∞-norms (see Table 1). The convergence rate is slightly better for the hexagonal than for the cartesian grid (see [10]). The EOC's for the unlimited second order schemes are as high as 2.6 for the coarsest grids, and drop slowly towards 2.0 as the grid is refined. In order to come to a practical conclusion, we compare the efficiency of the schemes as follows: given schemes A and B, we define the relative efficiency of the two schemes by

$$\mathcal{E} := \frac{cpu(B, h_*)}{cpu(A, h)}$$

where $cpu(A, h)$ is the CPU-time of scheme A on a grid with size h, h_* is the grid size on which scheme B obtains the same error as scheme A does with grid size h, and $cpu(B, h_*)$ is the respective CPU-time for scheme B. The break-even point is reached when $\mathcal{E} = 1$. It turns out that even though the unlimited third order schemes always give smaller errors than the unlimited second order schemes, they only become more efficient on very fine grids of about 160 points per period of the sine wave (see Table 2). For these grids, the error is already of order 10^{-6}. The limited third order schemes are less efficient than the limited second order schemes even on our finest grids (see Tables 3–4). Note that the cpu-time of the third order

o2g6 (no limiter)						
I	N	L^1	EOC	L^∞	EOC	scaled cpu
36	169	2.1052e-04	—-	3.7021e-04	—-	98.07
72	337	3.4710e-05	2.60	6.7174e-05	2.46	784.05
144	673	6.9411e-06	2.32	1.3937e-05	2.27	6280.46
288	1345	1.5672e-06	2.15	3.1576e-06	2.14	50453.16

o3g6 (no limiter)						
I	N	L^1	EOC	L^∞	EOC	scaled cpu
36	169	1.4185e-04	—-	2.3531e-04	—-	315.09
72	337	1.7806e-05	2.99	2.9578e-05	2.99	2517.94
144	673	2.2278e-06	3.00	3.7015e-06	3.00	20244.45
288	1345	2.7853e-07	3.00	4.6279e-07	3.00	161920.39

TABLE 1. Oblique sine wave, unlimited second order scheme o2g6 (top) and third order scheme o3g6 (bottom) on hexagonal grid. Direction of propagation $\theta = \arctan(1/(3\sqrt{3}))$. L^1- and L^∞-errors in the density, EOCs, and scaled cpu-times in seconds. I = number of points along one spatial period. N = number of timesteps.

schemes is about 3–4 times that of the second order one. This is reasonable, since for the third order scheme, four Gaussian quadrature nodes instead of one are needed for space-time accuracy.

Therefore even on this essentially trivial test problem our results seem to suggest that third order schemes, limited or unlimited, may be less efficient than second order schemes except for very fine grids. Therefore, the best chance to make the third order schemes competitive would be to use the structure of the piecewise quadratic reconstruction in order to relax the limiter near extrema of the solution more than it can be done for the piecewise linear scheme. In this case an essentially unlimited third order scheme would compete with a limited second order scheme, and such a third order scheme should be competitive on coarser grids as well.

Such a strategy has in fact been followed by Leonard and Niknafs [5], Liu and Osher [7] and Liu and Tadmor [9]. Leonard and Niknaf consider the one-dimensional constant coefficient scalar advection equation and use an ad-hoc-detector to distinguish physical from unphysical extrema. No limiting is applied to

I	18	36	72	144	288
I^*	16.2	31.5	57.6	98.6	161.9
$\mathcal{E}$	2.34	2.16	1.64	1.03	0.57

TABLE 2. Oblique sine wave, comparison of efficiencies of second and third order schemes on hexagonal grids based on L^1–errors (both schemes without limiter).

o2g6 (with limiter)						
I	N	L^1	EOC	L^∞	EOC	scaled cpu
36	168	7.1409e-04	—-	3.2072e-03	—-	105.82
72	337	1.7095e-04	2.06	1.1041e-03	1.54	853.27
144	673	3.7441e-05	2.19	3.7809e-04	1.55	5874.12
288	1345	7.9165e-06	2.24	1.2831e-04	1.56	47054.98

o3g6 (with limiter)						
I	N	L^1	EOC	L^∞	EOC	scaled cpu
36	168	4.1747e-04	—-	2.2786e-03	—-	324.58
72	337	9.2844e-05	2.17	7.5273e-04	1.60	2595.93
144	673	1.8779e-05	2.31	2.5019e-04	1.59	20776.73
288	1345	3.6277e-06	2.37	8.3013e-05	1.59	166560.07

TABLE 3. Same as Table 1, but limited schemes.

I	18	36	72	144	288
I^*	15.1	28.1	54.4	106.8	207.2
$\mathcal{E}$	1.80	1.45	1.31	1.44	1.32

TABLE 4. Same as Table 2, but limited schemes.

those extrema which are thought of being physical. Liu and Osher consider nonlinear scalar conservation laws. Since these equations satisfy a maximum principle, one can allow the spatial reconstruction at a given point to take values between the minima and maxima of the reconstruction in the previous timestep in the domain of dependence of this point. Liu and Tadmor consider one-dimensional scalar conservation laws as well as the system of the Euler equations. Since no pointwise maximum principle is known in this case they suggest, similarly as Leonard and Niknafs do, not to limit the extrema at all. This leads to a third order generalization of the Nessyahu-Tadmor scheme.

In the multidimensional system case which we considere here it is much harder to detect local extrema. Plane wave solutions, for example, are constant in the direction orthogonal to the direction of propagation. If there are now small numerical oscillations along the wavefront, then isolated extrema and saddle points will occur along the crest of the wave, making it hard for any scheme to detect the underlying physical wavefront.

In such situations, ENO and WENO reconstructions [2, 3, 8], which avoid the limiting procedure alltogether, have been rather successfull, and there are several higher than second order ENO codes for twodimensional flows.

scheme	h^{-1}	Density	EOC	Velocity	EOC	Pressure	EOC
o2g6	80	3.5436e-02	—	9.0276e-03	—	5.7925e-03	—
	160	1.9984e-02	0.83	4.5899e-03	0.98	2.8271e-03	1.03
o3g6	80	3.1829e-02	—	8.7064e-03	—	5.5383e-03	—
	160	1.8263e-02	0.80	4.4849e-03	0.96	2.7683e-03	1.00

TABLE 5. Oblique shocktube, averages of **global** L_1 errors over 24 directions. Second (o2g6) and third order (o3g6) schemes on hexagonal grid.

scheme	h^{-1}	Density	EOC	Velocity	EOC	Pressure	EOC
o2g6	80	2.1577e-03	—	1.5746e-03	—	1.0381e-03	—
	160	7.0850e-04	1.61	3.8556e-04	2.03	2.5277e-04	2.04
o3g6	80	2.0511e-03	—	1.4101e-03	—	9.5283e-04	—
	160	7.5074e-04	1.45	2.8799e-04	2.29	1.9584e-04	2.28

TABLE 6. Same as Table 5, but **local** errors and EOC's.

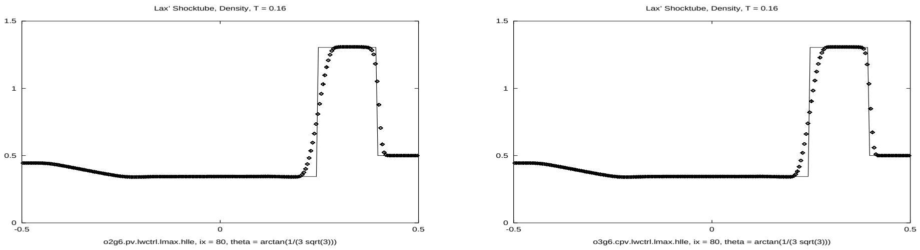

FIGURE 1. Lax' shocktube. Second order scheme o2g6 (left) and third order scheme o3g6 (right). Oblique flow across hexagonal grids, $h = \frac{1}{80}$, directions $\theta = \arctan(1/(3\sqrt{3}))$. Scatter plots of 2D solutions (2-3 cells in shock layer per 1D cross-section).

3.2. Oblique Lax' Shocktube

The next problem involves Lax' shocktube, computed in various directions obliquely to the grids. All schemes give satisfactory oscillation-free results similar to the one shown in Figure 1. The EOC's in the L^1-norm are about 0.8 in the density and about 1.0 in velocity and pressure (see Table 5). The errors are of the same order of magnitude for the third and second order schemes on cartesian and hexagonal grids, since they are dominated by the error in the discontinuity. We also study the **local** L^1-errors in regions of smooth flow and define a general procedure how to determine these regions automatically, see [10]. The EOC's are now between 1.5 and 1.7 for the density and between 1.9 and 2.3 for velocity and pressure, indicating the high order of accuracy of the schemes. However, the third

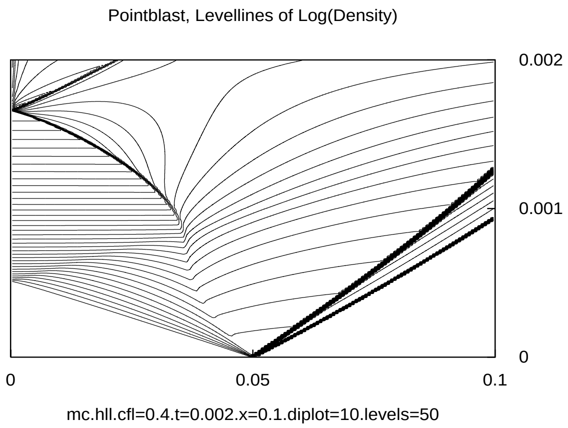

FIGURE 2. Radially symmetric pointblast. Levellines of $\log(\rho)$ in the $|x|$-t-plane. 50 equally spaced contours. One-dimensional operator-splitting scheme with CFL = 0.4. and 1200 points.

o2g6.pv.lmax.lwctrl.hll: global errors						
I	Density	EOC	Velocity	EOC	Pressure	EOC
40	1.7100e-01	—-	2.3159e-01	—-	1.3826e-01	—-
80	1.1483e-01	0.57	1.1897e-01	0.96	7.2169e-02	0.94
160	7.4305e-02	0.63	6.4683e-02	0.88	4.7644e-02	0.60
320	4.2746e-02	0.80	3.1937e-02	1.02	2.6523e-02	0.85

o3g6.cpv.lmax.lwedge.hll: global errors						
I	Density	EOC	Velocity	EOC	Pressure	EOC
40	1.4520e-01	—-	2.3395e-01	—-	1.2815e-01	—-
80	9.3089e-02	0.64	1.1333e-01	1.05	5.9385e-02	1.11
160	6.0728e-02	0.62	6.0344e-02	0.91	3.8452e-02	0.63
320	3.5418e-02	0.78	2.9496e-02	1.03	2.1034e-02	0.87

TABLE 7. Radially symmetric pointblast, time $T = 0.002$, second and third order schemes on hexagonal grids. **Global** errors and EOCs.

order schemes do not perform significantly better than the second order ones, and neither do those on hexagonal grids when compared to schemes on cartesian grids.

3.3. Radially Symmetric Pointblast

We go on to more challenging test problems. For a radially symmetric strong blast wave (see Figure 2) which was used by LeVeque and Walder [6], the four schemes

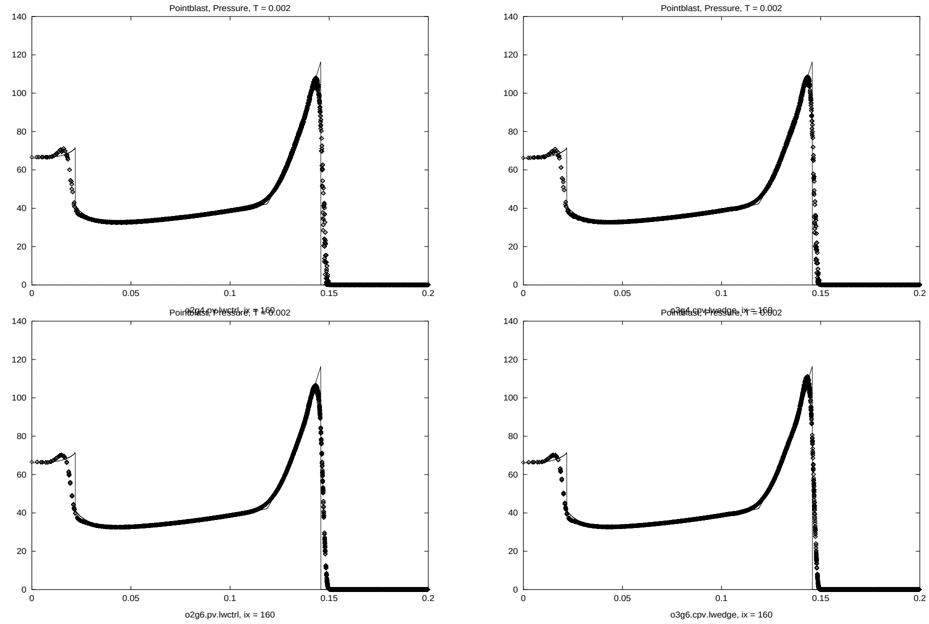

FIGURE 3. Radially symmetric pointblast. Pressure at time $T = 0.002$. Scatter plots of 2D solutions (2-3 cells in shock layer per 1D cross-section). Second order schemes (left column) and third order schemes (right column) in primitive variables. Cartesian (top) and hexagonal grids (bottom), $I = 160$. The solid line is the 1D solution with 12800 points.

o2g6.pv.lmax.lwctrl.hll: local errors						
I	Density	EOC	Velocity	EOC	Pressure	EOC
40	3.0095e-02	—-	5.1056e-02	—-	2.6050e-02	—-
80	1.0216e-02	1.56	1.8052e-02	1.50	9.9409e-03	1.39
160	1.9380e-03	2.40	8.2650e-03	1.13	2.8387e-03	1.81
320	3.0509e-04	2.67	4.0380e-03	1.03	1.0581e-03	1.42

o3g6.cpv.lmax.lwedge.hll: local errors						
I	Density	EOC	Velocity	EOC	Pressure	EOC
40	2.3748e-02	—-	5.8163e-02	—-	2.1475e-02	—-
80	6.2397e-03	1.93	2.0769e-02	1.49	7.5236e-03	1.51
160	9.9778e-04	2.64	8.4130e-03	1.30	1.9825e-03	1.92
320	1.5251e-04	2.71	3.9418e-03	1.09	8.0392e-04	1.30

TABLE 8. Same as Table 7, but **local** errors and EOCs.

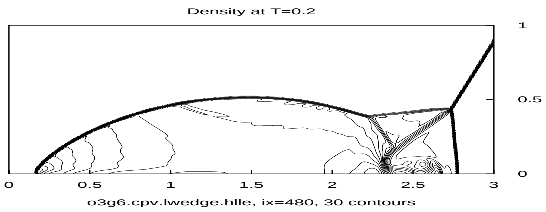

FIGURE 4. Double Mach Reflection, density, $h = \frac{1}{120}$. From top to bottom: Second and third order schemes on cartesian grid and second and third order schemes on hexagonal grid.

produce almost perfectly radially symmetric solutions (in this case the schemes on hexagonal grids are somewhat superior, see Figure 3). We carefully evaluate global and local L^1-errors by comparing the two-dimensional solutions with that of a resolved one-dimensional calculation (see Tables 7–8). Again, the second and third order schemes produce comparable errors. For more details, see [10].

3.4. Double Mach Reflection

The last problem which we consider is the double Mach reflection. In Figure 4 we show levelplots of the density computed by the third order scheme on hexagonal grids. The gridsize is given by $h = \frac{1}{120}$. All other schemes produce comparable results [10].

The schemes capture the shocks, contact discontinuities and the jet equally well. In the region bounded by the second Mach shock, the curved reflected shock, and the reflecting wall they all exhibit the slight oscillations which are typical of MUSCL-type schemes. Once more, the second order scheme on cartesian grids, which requires the least amount of cpu-time and computer storage, is the most efficient one for this problem.

4. Conclusion

In all the computations presented above, the limited third order TVD-type finite volume scheme was less efficient than the corresponding second order scheme. At this point, however, this conclusion can only be seen as preliminary. The key issue which decides over the success of any MUSCL-type scheme is the limiting procedure for the spatial reconstruction. In future work, we will explore whether a further weakening of the limiting procedure described in Section 2 will make the third order scheme competitive. In particular, we will experiment with Shu's TVB technique [12], which introduces an additional parameter into the scheme. Recently, Cockburn and Shu used this concept successfully in the context of the Runge-Kutta Discontinuous Galerkin method [1].

References

[1] B. Cockburn and C.-W. Shu, *The Runge-Kutta local discontinuous Galerkin finite element method for conservation laws V: Multidimensional systems.* ICASE-Report 97-433 (1997). To appear in J. Comput. Phys.

[2] A. Harten, B. Engquist, S. Osher and S. Chakravarthy, *Uniformly high-order accurate essentially non-oscillatory schemes III.* J. Comput. Phys. 71 (1987), 231–303.

[3] G.-S. Jiang and C.-W. Shu, *Efficient implementation of weighted ENO schemes.* J. Comput. Phys. 126 (1996), 202 – 228.

[4] B.P. Leonard, *The ULTIMATE conservative difference scheme applied to unsteady one-dimensional advection.* Comp. Meth. Appl. Mech. Eng. 88 (1991), 17–74.

[5] B.P. Leonard and H.S. Niknafs, *Sharp monotonic resolution of discontinuities without clipping of narrow extrema.* Computers & Fluids 19 (1991), 141–154.

[6] R.J. LeVeque and R. Walder, *Grid alignment effects and rotated methods for computing complex flows in astrophysics.* eds. J.B. Vos, A. Rizzi and I.L. Rhyming, Proceedings of the Ninth GAMM Conference on numerical methods in fluid mechanics. Notes Num. Fluid. Mech. 35 (1992), 376–385.

[7] X.-D. Liu and S. Osher, *Nonoscillatory high order accurate self-similar maximum principle satisfying shock capturing schemes I.* SIAM J. Numer. Anal. 33 (1996), 760–779.

[8] X.-D. Liu, S. Osher and T. Chan, *Weighted essentially non-oscillatory schemes.* J. Comput. Phys. 115 (1994), 200–212.

[9] X.-D. Liu and E. Tadmor, *Third order nonoscillatory central scheme for hyperbolic conservation laws.* Preprint 1996.

[10] S. Noelle, *High order finite volume schemes for the two-dimensional compressible Euler equations.* Habilitationsschrift, Universität Bonn, Germany (1997).

[11] R. Sanders, *A third-order accurate variation nonexpansive difference scheme for single nonlinear conservation laws.* Math. Comp. 51 (1988), 535–558.

[12] C.-W. Shu, *TVB uniformly high order schemes for conservation laws.* Math. Comp. 49 (1987), 105-121.

Institute of Applied Mathematics,
Bonn University,
Wegeler Str. 10,
53115 Bonn, Germany.
Supported by DFG-SFB256 grant at Bonn University.
E-mail address: `noelle@iam.uni-bonn.de`